BULLETIN OF THE POLISH ACADEMY OF SCIENCES
TECHNICAL SCIENCES, Vol. 71(6), 2023, Article number: e148250
DOI: 10.24425/bpasts.2023.148250

Turbine wheel reduced modal model for self-excited vibration suppression by inter-blade dry-friction damping

Luděk PEŠEK*, Pavel ŠNÁBL, and Chandra Shekhar PRASAD

Institute of Thermomechanics of the CAS, v. v. i., Dolejškova 1402/5, 182 00 Praha 8, Czech Republic

Abstract. A new approach to calculations based on the modal synthesis method is proposed for the evaluation of structural and dry-friction damping effects on self-excited vibrations due to aeroelastic instability in bladed turbine wheels. The method described herein is used to study dry-friction damping of self-excited vibration of an industrial turbine wheel with 66 blades. For evaluating damping effects, the blade couplings are applied to this particular turbine wheel. Therefore, neighbouring blades are interconnected by rigid arms that are fixed on one side to one blade and are in frictional contact on their free side with the other blade. Due to relatively normal motions in contacts, the prescribed contact forces vary over time. The aerodynamic excitation arises from the spatially periodical flow of steam through the stator blade cascade. In this paper, we attempt to model flow-induced instabilities with the Van der Pol model linked to relative motion between neighbouring blades. The proposed modal synthesis method as ROM is a computationally efficient solution allowing substantial parametrization. The effect of the angles of contact surfaces on the wheel dynamics and on the level of the self-excitation suppression will be discussed herein.

Key words: blade dynamics; travelling waves; flutter; dry-friction damping; model reduction; Van der Pol.

1. INTRODUCTION

The trend in the development of power turbines and jet engines is to continuously improve performance and energy efficiency. With thinner, lighter and high-aspect ratio blades in the LP stage of a steam turbine, the dynamic effect of steam on the blades becomes a controlling factor in the aeroelastic stability of a blade. The research on these physical phenomena is based on modern computational methods and experimental studies of the dynamics of rotating blade wheels and the unsteady flow in blade cascades.

In the case of flutter instability, the higher-level vibration is caused by aeroelastic coupling between the blades and a flow field. According to flow distortion and its volumetric rate around the blade airfoil, the different types of self-excited vibration occur synchronously or non-synchronously with respect to the rotation frequency. These states in full operational range are more difficult to predict. A bladed wheel with sufficient dissipation of mechanical energy protects against this. Since the material damping of the metal blades is very low, it is necessary to increase the damping by additional construction damping, namely dry-friction damping. Dry-friction damping can be introduced into the turbine design [1] by couplings in roots, shrouds or platforms of the blades.

1.1. Dry-friction damping

Dry-friction damping in bladed discs in combination with their mistuning or at travelling wave deformation modes was studied already in the 80s [2–4]. The influence of friction damping on the dynamic behaviour of the blading is, however, a complex nonlinear problem of continuum mechanics relating to the dynamic behaviour of spatially distorted blades coupled by disk and time-variant boundary conditions at contacts with friction [5].

The first papers on finite element methods as applied to contact problems appeared in the 70s [6]. Since then, much literature on linear and complex nonlinear contact approaches under the FEM has appeared [7, 8]. Nonlinear contact couplings [9–11] are influenced by production accuracy, roughness of the contact surfaces, thermomechanical coupling, etc.

There are different approaches to this problem, ranging from analytical models with several degrees of freedom [12–14] to numerical spatial 3D finite element models [15–19]. Friction is described here from a phenomenological point of view. The general Coulomb's law is commonly used to describe the frictional forces in contacts, where the friction coefficient is a function of the relative velocity and the quality of the surfaces. The contact friction model can be simplified for stationary harmonic oscillations by linearizing the nonlinear contact forces using the harmonic balance method (HBM) [20]. HBM is very well-developed theoretically and computationally very efficient in the dynamics of bladed disks with frictional contacts [21–27].

The other methods for solution of dynamics of bladed discs with dry-friction contacts are based on the reduced order models (ROM), where the linear blades and discs are reduced, e.g.,

*e-mail: pesek@it.cas.cz

Manuscript submitted 2023-04-26, revised 2023-10-18, initially accepted for publication 2023-10-30, published in December 2023.

by modal synthesis method, to small numbers of DOFs, and the non-linearity remains only in contacts [28, 29].

New methods of computational contact mechanics based on finite element technology are still under investigation. Here, contact forces are calculated using e.g., Penalty, Lagrangian or Augmented Lagrangian methods. These methods are usable for general dynamic excitation with smooth and non-smooth contact surfaces since the bladed disc dynamics with non-holonomic contact constraints are solved as a discretized fully-coupled nonlinear problem in a time domain. However, this solution tends to lead to a need for high-performance computing (HPC) [30].

1.2. Flutter phenomena

As to the flutter stability of LP turbine, it dominates the design characteristics and is the subject of much attention [31–33] to ensure uninterrupted and safe power production in nuclear power plants. The unsteady phenomenon of flutter occurs when the sum of mechanical damping of the blades and aerodynamic damping of the airflow becomes zero. At this point, the blades experience severe self-excited vibrations that reduce turbine efficiency and increase blade fatigue damage. Flutter in steam turbine LP stages is a very complex physical phenomenon, and to date the fundamental physics behind is not fully understood, so it remains a very active topic of research [34–37].

Numerically, it is linked with solving fluid and structure domains and their interaction. The solution is very computationally costly by use of standard discretisation methods, e.g. CFD-CSD numerical tools. Though CFD-CSD model yields quite accurate estimations and manages to capture the complex physics of blade-flow interaction, these tools are computationally very expensive and demand advance computing infrastructures to execute. This can be observed in the work of [38–40], where each of the researchers has employed conventional CFD-RANS/URANS flow solvers loosely coupled with FEM-structural solvers to estimate the aerodynamic damping of turbine blade cascade. In the first step, a FEM-based structural solver was employed to determine the mode shape and frequency of the blade which then was fed as an input to the transient CFD-solver for aerodynamic damping estimation. In this method, the flow fields around one or more blade channels are discretised using FV elements to be used in CFD-solver.

Therefore, in a quest to reduce the computational cost in the preliminary design phase, a new reduced order of aeroelastic model (ROAM) approaches arises. Using ROAM numerical methods is a good compromise of speed and accuracy. In the recent past, ROAM has gained noticeable popularity in field of turbomachinery flutter modelling in both industrial and academic research. ROAMs have been adopted by many researchers, e.g., panel method [41–45]. In one of the most recent works [45] the ROAM approach was used to model aeroelastic stability problem in turbomachinery. In this work, ROAM for uncoupled and coupled flutter analysis in cascade was employed and has demonstrated a significant reduction in computational time without compromising the accuracy of the solution. However, in both the uncoupled and coupled ROAM models the unsteady aerodynamic load is estimated using a time-linearised CFD-model, which can make this ROAM approach slower for large 3D models. Therefore, to further reduce the computational cost of ROAM model, a boundary element method (BEM) based ROAM model for turbomachinery blade flutter estimation was proposed recently [43]. It has employed the BEM-based ROAM to model the aeroelastic stability parameters in annular cascade and compared the results against CFD-CSD based models. The results show a significant reduction in computational time.

Furthermore, in [46], a posterior alternative method called the Tie-Dye (TD) method was proposed to quickly check the influence of mode shape and the reduced frequency on the stability characteristics of the LP-stage blade cascade in the preliminary design stage. Since then, the TD method has been used reliably by a number of researchers and industrial designers for the quick estimation of aeroelastic stability of the system for both subsonic and supersonic cascade flow [33, 47]. However, the TD method itself requires either time or frequency domain CFD analyses to create a TD map for each blade geometry, so it can take longer to create the TD map for different blade geometries. Consequently, the overall computational cost can be higher than those harmonic balancing (HB), or frequency domain methods, and it is definitely slower then BEM-based ROAM [43]. Therefore, it can be safely said that ROAM methods are more suitable for numerical flutter analysis at a preliminary design stage and can be used in industrial research.

To support and validate the numerical research, experiments are still needed. Similarly to the numerics, where the models are reduced as explained above, also in the experiments a certain level of simplification is needed to allow the measurements that would hardly be possible in a real rotating turbine wheel. Although there are researchers that work with the annular cascade design [48], which respects the geometry of the bladed wheel, most of the researchers use so-called linear cascades with prismatic blades that respect the cross-cut at a certain diameter of the bladed wheel. Because the flutter phenomenon is a very complex problem - each research team usually focusing only on a specific region of interest in terms of flow and mechanical conditions. Some experiments have blades with two degrees of freedom [49, 50], corresponding to blade bending and torsion, some focus only on blade bending [51] and some only on blade torsion [52]. The flow velocities in the experiments range from subsonic [49, 50] to transonic [51, 52].

1.3. Flutter suppression by dry-friction damping

As shown in previous subsections, the solutions themselves of either dry friction damping or flutter in turbine wheels are very complex and are still under development. Therefore, there are approaches to simplify the numerical solutions by ROM modelling to bring it into their practical design tools. The solution of both phenomena together is even more challenging.

Therefore, recently [53, 54], a new calculation approach based on the modal synthesis method [55] was proposed for evaluation of dry-friction damping effects on self-excited vibrations induced by aeroelastic forces in the bladed wheels where tie-boss and shroud couplings are applied (Fig. 1).

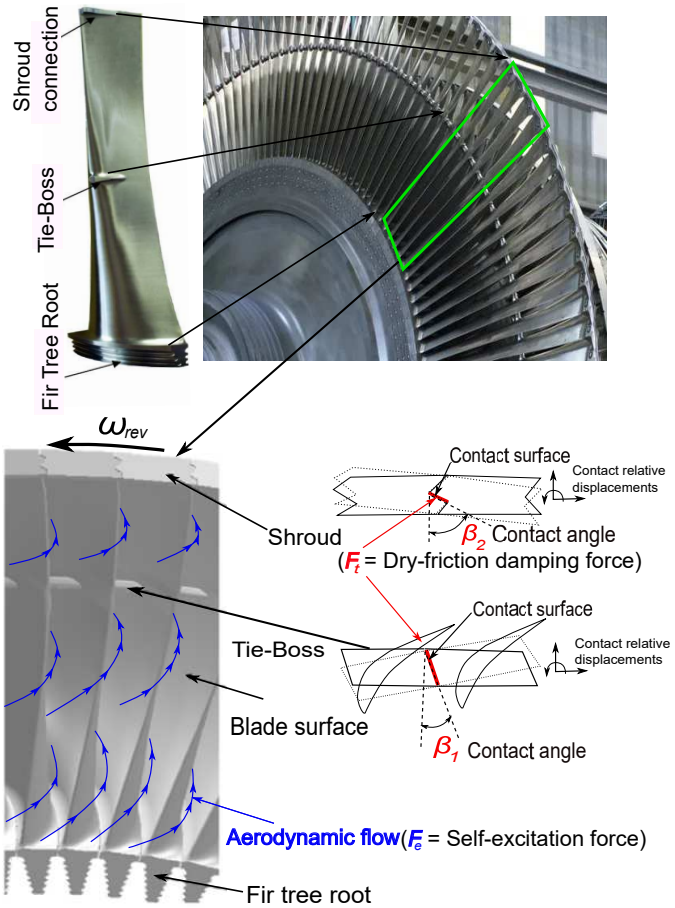

Fig. 1. Schematic picture of the aeroelastic forces and frictional elements

To simplify the model of inter-blade couplings, neighbouring blades are interconnected by rigid arms that are on one side fixed to one blade and are in frictional contact on their free side with the other blade. Static normal contact forces are prescribed in contact point pairs in the initial state. Due to relative normal motions in contacts, the prescribed contact forces vary over time. Frictional force in contacts is dependent on contact surface angles and is driven by the modified Coulomb's friction law.

The aerodynamic excitation arises from the spatially periodical flow of steam through the stator blade cascade. The self-excited aeroelastic forces of blades were described by the Van der Pol model [56]. In [54], we considered the Van der Pol model linked to the absolute motion of the blades. The simulations, however, showed that no angle of contact surfaces can prevent the onset of flutter. Therefore, in this paper, we will aim at the effect of Van der Pol model linked instead of absolute motion of blades to relative motion between them. From the point of view of the theory of flutter of blade cascades, this type of motion can also play an important role in the occurrence of flutter.

In general, the use of modal synthesis as a ROM method is based on the assumption that the forced vibration response of the turbine blade wheel is quasi-linear, and nonlinearity enters the equation of motion only by self-excitation described by the Van der Pol damping model, which can increase the vibration amplitudes very quickly. If the amplitudes reach high values and the material and geometrical linear limits are exceeded, this assumption would be violated. However, the aim of this approach is to study the effect of dry friction on the suppression of high amplitudes, where dry friction acts on the vibration at a very early stage of self-excitation and the level of amplitudes is kept at relatively low levels, so that this assumption is satisfied.

The proposed method as ROM is a computationally efficient solution allowing a parametric optimization, for example, contact surface angles, of a complex nonlinear mechanical system. The paper will be aimed at the narrow frequency range of excitation and on the case when a slip motion in the contacts prevails. The effect of the angles of contact surfaces on the wheel dynamics and on the level of the self-excitation suppression will be discussed for the modified Van der Pol model.

2. VAN DER POL MODELS OF SELF-EXCITATION IN BLADES TURBINE CASCADE

Steam flowing through the rotating blade cascade can cause a decrease of damping and aeroelastic flutter instability. Since an exact description of this aeroelastic phenomenon is very complicated [32, 33], we proposed the Van der Pol model [57]. There are two types of the aerodynamic forces:

1. The velocity of steam flowing from the stator cascade has a periodic profile due to the stator blades distortion, and the wakes of flow from the stator blades produce forced vibration of the rotating blades. Varying numbers of blades of rotor and stator wheels cause phase delays of excitation forces produced by these wakes.
2. The flowing steam through the rotating blade cascade produces, besides the aforementioned periodic forced vibration, vertical and torsional aeroelastic self-exciting forces.

Both of these sources of excitation interact mutually, and the running waves of forced vibration initiate the flutter running waves. The proposed Van der Pol models can describe two aerodynamic effects: the first acting on individual blades controlled by only one blade's motion and the second acting on neighbouring blades controlled by relative motions of the blades. For 1DOF profile with vertical motion (Fig. 2), the first form of the Van der Pol model is described by the equation

$$G_i = -\mu_0 \left(1 - \left(\frac{y_i}{r}\right)^2\right) \dot{y}_i \tag{1}$$

and the other by

$$F_{e,i} = -\mu_1 \left(1 - \left(\frac{y_i - y_{i-1}}{r}\right)^2\right) (\dot{y}_i - \dot{y}_{i-1}) + \\ + \mu_1 \left(1 - \left(\frac{y_{i+1} - y_i}{r}\right)^2\right) (\dot{y}_{i+1} - \dot{y}_i), \tag{2}$$

where G_i, $F_{e,i}$ are the aerodynamic forces, y_i, $\dot{y}_i$ are vertical displacement and velocity of blade i, r is the amplitude at which

the negative damping changes to positive. This property allows us to study the behaviour in the unstable regions because it prevents the amplitude from growing to infinity. The values μ_0 and μ_1 give the intensity coefficients of the Van der Pol models. Equation 2 describes force couplings of the blade i with motions of neighbouring blades $i-1$, $i+1$. The stiffness and viscous damping in direction y is k and b. The aerodynamic forces act in aerodynamic centre O.

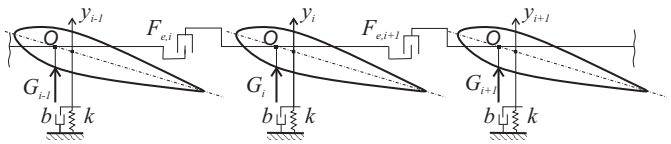

Fig. 2. Section of a blade cascade

3. MODAL SYNTHESIS METHOD

The modal synthesis method comes from the coupling of subsystems defined in modal space. The homogeneous equation of motion of the undamped subsystem can be written in matrix form as

$$\mathbf{M}\ddot{\mathbf{u}} + \mathbf{K}\mathbf{u} = \mathbf{0}, \tag{3}$$

where $\mathbf{M}$ and $\mathbf{K} \in \mathbb{R}^{n\times n}$ are square mass and stiffness matrices of dimension n, $\ddot{\mathbf{u}}$, $\mathbf{u}$ are acceleration, displacement vectors of the DOFs.

Which leads to the eigenvalue problem

$$(\mathbf{K} - \mathbf{\Lambda M})\mathbf{X} = \mathbf{0}. \tag{4}$$

The solution of equation (2) yields the matrices of eigenvalues $\mathbf{\Lambda}$ and eigenvectors $\mathbf{X}$

$$\mathrm{Diag}(\mathbf{\Lambda}) = [\lambda_1, \lambda_2, \ldots, \lambda_n], \quad \mathbf{X} = [\mathbf{x}_1, \mathbf{x}_2, \ldots, \mathbf{x}_n]. \tag{5}$$

If the eigenvector matrix satisfies the orthonormal condition, then

$${}^{\mathrm{T}}\mathbf{X}\mathbf{M}\mathbf{X} = \mathbf{I}, \quad {}^{\mathrm{T}}\mathbf{X}\mathbf{K}\mathbf{X} = \mathbf{\Lambda}. \tag{6}$$

The homogenous equation of motion of a global system composed of subsystems is

$$\mathbf{M}_c\ddot{\mathbf{u}}_c + \mathbf{K}_c\mathbf{u}_c = \mathbf{0} \tag{7}$$

where $\mathbf{M}_c$, $\mathbf{K}_c$ are global mass and stiffness matrices and $\mathbf{u}_c$ displacement with eigenvalue characteristics $\mathbf{\Lambda}_c$, $\mathbf{X}_c$. Matrices $\mathbf{K}_c$, $\mathbf{M}_c$, $\mathbf{X}_c$, $\mathbf{\Lambda}_c \in \mathbb{R}^{nn_r\times nn_r}$ (n is the number of DOFs of the segment, n_r is the number of segments).

To couple the subsystems in global matrices, we must create a coupling between them. Each connection between the blade subsystems can be described by a constraint vector $\mathbf{T}_v$. To create the full modification stiffness matrix in the original DOFs, the constraint can be expressed by a constraint vector $\mathbf{T}_v$ and stiffness of connection c_1 as in [56]

$$c_1\,{}^{\mathrm{T}}\mathbf{T}_v\mathbf{u}_c = F_1. \tag{8}$$

Then the modification stiffness is constituted as

$$\Delta\mathbf{K} = \mathbf{T}_v\,{}^{\mathrm{T}}\mathbf{T}_v c_1. \tag{9}$$

The full synthesized system can be described by the equation of motion

$$\mathbf{M}_c\ddot{\mathbf{u}}_{cN} + (\mathbf{K}_c + \Delta\mathbf{K})\,\mathbf{u}_{cN} = \mathbf{f}_{cE}, \tag{10}$$

which leads to the eigenvalue problem

$$(-\mathbf{\Lambda}_{cN}\mathbf{M}_c + (\mathbf{K}_c + \Delta\mathbf{K}))\,\mathbf{X}_{cN} = \mathbf{0}. \tag{11}$$

To reduce the full DOF space of the synthesized structure equation (9), we chose the modal subspace

$$\overline{\mathbf{X}}_c = \begin{bmatrix} \overline{\mathbf{X}} & 0 & 0 & 0 \\ & \overline{\mathbf{X}} & 0 & 0 \\ sym & & \ldots & 0 \\ & & & \overline{\mathbf{X}} \end{bmatrix},$$

where $\overline{\mathbf{X}} \in \mathbb{R}^{n\times m}$ is matrix of m arbitrarily-chosen eigenvectors of $\mathbf{X} \in \mathbb{R}^{n\times n}$ of the original one-blade subsystem. Introducing the transformation $\mathbf{u}_{cN} = \overline{\mathbf{X}}_c\mathbf{Q}_{cNR}\mathbf{u}_R$ and $\ddot{\mathbf{u}}_{cN} = -\overline{\mathbf{X}}_c\mathbf{\Lambda}_{cNR}\mathbf{Q}_{cNR}\ddot{\mathbf{u}}_R$ and pre-multiplying by ${}^{\mathrm{T}}\overline{\mathbf{X}}_c$ in equation (8), when the eigenvector matrix $\overline{\mathbf{X}}_c$ satisfies the orthonormal condition given by equation (4), leading to a new eigenvalue problem

$$[-\mathbf{\Lambda}_{cNR} + (\mathbf{\Lambda}_{cR} + \Delta\mathbf{K}_{cR})]\,\mathbf{Q}_{cNR} = \mathbf{0}. \tag{12}$$

where $\Delta\mathbf{K}_{cR} = {}^{\mathrm{T}}\overline{\mathbf{X}}_c\Delta\mathbf{K}\overline{\mathbf{X}}_c$ is the reduced modification matrix of $\mathbb{R}^{mn_r\times mn_r}$. The calculated eigenvector matrix $\mathbf{Q}_{cNR}$ is a transform matrix between the modal subspace $\overline{\mathbf{X}}_c$ and a modal matrix of the reduced system.

In steam turbines the stator blades create so-called nozzle excitation, i.e., a spatially periodical flow that acts on the rotor blades with a periodic force whose frequency is dependent on angular velocity of the rotor and number of stator blades. The number of stator blades is usually chosen to be lower than the number of rotor blades, and their difference gives the number of nodal diameters (ND), which are excited by the nozzle excitation. The excitation force can be described by

$$F_{Ei} = F_b\cos\left[n_s\omega_r t - 2\pi\left(1 - \frac{n_s}{n_r}\right)i\right], \quad i = 1,\ldots,n_r, \tag{13}$$

where F_b is the force amplitude, ω_r the angular velocity of the rotor and n_r and n_s are the numbers of rotor and stator blades.

In addition to nozzle excitation, we assumed the Van der Pol self-excitation aerodynamic forces in equation (2) that uniformly act on one selected mode of each blade

$$F_{e,i} = -\mu_1\left(1 - \left(\frac{u_{RBi} - u_{RBi-1}}{r}\right)^2\right)(\dot{u}_{RBi} - \dot{u}_{RBi-1}) + \\ + \mu_1\left(1 - \left(\frac{u_{RBi+1} - u_{RBi}}{r}\right)^2\right)(\dot{u}_{RBi+1} - \dot{u}_{RBi}), \\ i = 1,\ldots,n_r, \tag{14}$$

where u_{RBi} displacements and $\dot{u}_{RBi}$ velocities of defined modal coordinates are calculated for each blade at each step of time integration.

To preserve the solution in modal space, the external and self-excitation forces must then be expressed in reduced space as well, so force vector ${}^{\mathrm{T}}\mathbf{f}_{cRE} = \left[{}^{\mathrm{T}}\mathbf{f}_{cRE1} \quad {}^{\mathrm{T}}\mathbf{f}_{cRE2} \quad \ldots \quad {}^{\mathrm{T}}\mathbf{f}_{cREn}\right]$ of the nozzle excitation is composed of reduced external excitation vectors $\mathbf{f}_{cREi} = \mathbf{p}_{Ei}F_{Ei}$ of each blade ($i = 1,\ldots,n_r$), where $\mathbf{p}_{Ei} = {}^{\mathrm{T}}\overline{\mathbf{X}}\mathbf{d}_{cEi}$ is participation factor of i-blade. Distribution excitation vector $\mathbf{d}_{cEi}$ of the blade is the zero vector with unit values only on positions corresponding to the DOFs of the blade where forces act.

The construction of the self-excitation vector $\mathbf{F}_e$ is analogous to $\mathbf{f}_{cRE}$. The corresponding participation vectors designated for this case as $\mathbf{p}_i$ blades is multiplied by function equation (14). Assuming uniformity of the self-excitation distribution along the blades, the self-excitation vectors $\mathbf{d}_{ci}$ are set to unity.

Then equation of motion of the synthesized reduced wheel system can be expressed as

$$\mathbf{M}_{cR}\ddot{\mathbf{u}}_R+\beta_D(\mathbf{K}_{cR}+\Delta\mathbf{K}_{cNR})\dot{\mathbf{u}}_R+\mathbf{F}_e(\mathbf{u}_{RB},\dot{\mathbf{u}}_{RB})+ \\ +(\mathbf{K}_{cR}+\Delta\mathbf{K}_{cNR})\mathbf{u}_R=\mathbf{f}_{cRE}(t)+\mathbf{f}_{cRt}(t), \quad (15)$$

where $\mathbf{K}_{cR} = {}^{\mathrm{T}}\overline{\mathbf{X}}_c\mathbf{K}_c\overline{\mathbf{X}}_c$, $\mathbf{M}_{cR} = {}^{\mathrm{T}}\overline{\mathbf{X}}_c\mathbf{M}_c\overline{\mathbf{X}}_c$, β_D is the coefficient of proportional damping and $\mathbf{f}_{cRt}$ the contact forces due to tie-boss and shroud couplings.

4. FRICTION CONTACT MODEL

The kinematics of the relative displacements of profiles 1 and 2 at the contact point is shown in Fig. 3.

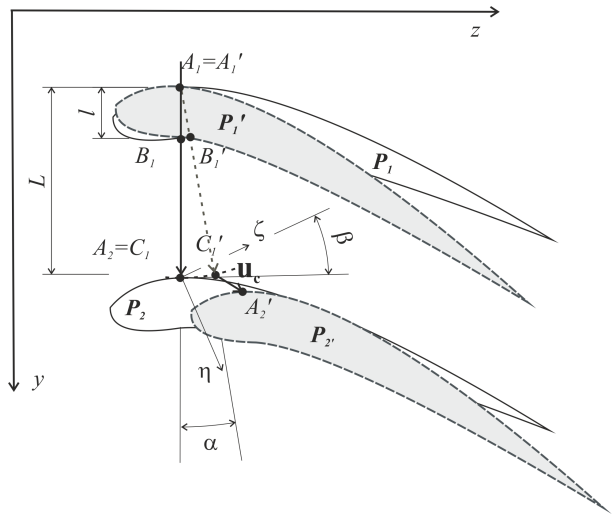

Fig. 3. Kinematics of relative displacement between contact pair C_1, A_2 of blade profiles P_1, P_2, respectively

Generally, the blade i has a profile cross-section P_i with arm placement height H. The profile P_i is interconnected with P_{i+1} of the neighbouring blade by the arm described by vector $\overrightarrow{A_iC_i}$ of length L. The arm is fixed with the profile P_i. The contact pairs of two neighbouring profiles consist of point C_i and point A_{i+1} lying on the upper edge of the profile P_{i+1}, these points overlap in an undeformed state of cascade. With the deformation of blades, profiles displace and rotate to P_i' and P_{i+1}' (shaded areas). By rotating the rigid arm A_iC_i by angle α given by rotation of profile P_i, we get the new position of C_i designated as C_i'.

Since the initial positions of points A_i, B_i and their displacements $\mathbf{u}_{Ai}$, $\mathbf{u}_{Bi}$

$$A_i = [x_{Ai}, y_{Ai}, z_{Ai}],\ \mathbf{u}_{Ai} = [u_{xAi}, u_{yAi}, u_{zAi}]$$
$$B_i = [x_{Bi}, y_{Bi}, z_{Bi}],\ \mathbf{u}_{Bi} = [u_{xBi}, u_{yBi}, u_{zBi}]$$

define deformed positions A_i', B_i' in the global coordinate system GCS (x, y, z), we can evaluate a deformed position of point C_i by prolongation of the vector $\overrightarrow{A_i'B_i'}$. Then, coordinates of C_i' can be expressed as

$$C_i' = A_i' + \vec{a}_{A'B'} \cdot L, \quad (16)$$

where $\vec{a}_{A'B'}$ is direction unit vector of $\overrightarrow{A_i'B_i'}$. The total relative displacement in contact pair can be simply expressed as

$$\mathbf{u}_c = A_{i+1}' - C_i'. \quad (17)$$

In defining a plane of the sliding of each contact pair, we introduce a local coordinate system LCS (ξ_i, η_i, ζ_i) in the initial state $C_i = A_{i+1}$ of the contact points when a normal vector $\vec{n}_i$ of the contact surface lies on axis η_i. Since axis x is identical with axis ξ, a relative motion in the contact will be possible only in directions ξ, ζ, and the transformation of displacement $\mathbf{u}_c$ from GCS to LCS is gained just by use of the rotation matrix $\mathbf{T}_{g2l}$ given by angle β between axes y, z and η, ζ as

$$\overline{\mathbf{u}}_{c,i} = \mathbf{T}_{g2l}\mathbf{u}_{c,i} = \begin{bmatrix} 1 & 0 & 0 \\ 0 & \cos\beta_i & \sin\beta_i \\ 0 & -\sin\beta_i & \cos\beta_i \end{bmatrix} \begin{bmatrix} u_{cx,i} \\ u_{cy,i} \\ u_{cz,i} \end{bmatrix}. \quad (18)$$

The slip velocity $v_{cj,i}$ ($j = \eta,\ \zeta$) in the contact is calculated from relative displacements of contacts as

$$v_{cj,i} = \frac{d\overline{u}_{cj,i}}{dt}.$$

The modified Coulomb frictional force of each contact pair i placed between the blades i and i+1 is depicted in Fig. 4. The F_{ts}, F_{td} are static and dynamic Coulomb frictional forces, respectively,

and v_k defines the length of the interval of total slip velocity v_c in which the Coulomb frictional force discontinuity is approximated via a steep straight line (micro-slip phase) [13, 14].

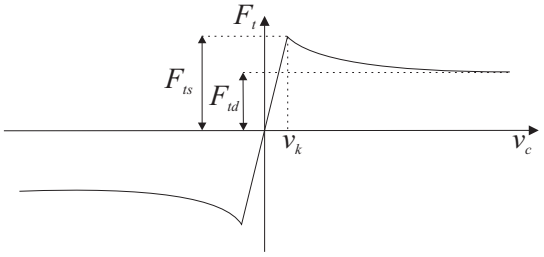

Fig. 4. Dependence of frictional force on relative velocity in the contact

The normal displacements in the contacts cause a change in the normal contact forces and stiffness in the contact. This stiffness is estimated from the blade stiffness calculated as an influence coefficient in the contact point and inter-blade connecting arm depending on contact surface angles β_i. For this purpose, the model of one blade in ANSYS was loaded with unit forces in both contact points in global coordinates y and z and the stiffness was evaluated from the deformation of the blade for both arms. Transformation into the normal direction was then used based on the surface angles. The resulting stiffness is shown in Fig. 5.

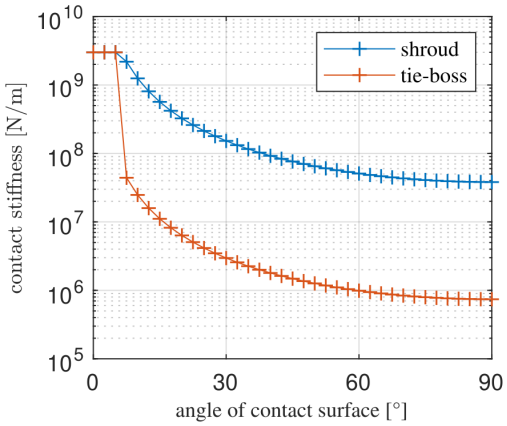

Fig. 5. Dependence of contact stiffness k_c on the angle of contact surface β

At the angles $\beta = 90°$, stiffness reaches minimal values. At those angles, the normal contact force is perpendicular to tie-boss arm axis. As the angles approach zero, the level of normal contact forces that loads the blade with torque becomes continually smaller, and the stiffness of the arms prevails. Since tie-boss arms are much stiffer than the blades, the total stiffness for $\beta = 0°$ goes to high values (corresponding to the stiffness of tie-bosses) because the normal forces act in the tie-boss axis. Therefore, tie-boss axial stiffness was used to set the stiffness values around zero angles of $\beta_{i,2}$. The time-varying normal contact forces were calculated as

$$F_{n,i} = \overline{F}_{t\eta,i} = F_{N0} - k_c \bar{u}_{c\eta,i} \tag{19}$$

where η is the normal direction of the contact surfaces, F_{N0} the initial value of normal force in contacts. The normal forces in equation (19) were, together with frictional forces, in directions $j = \xi,\ \zeta$ for each contact pair i transformed to GCS by transposed matrix $\mathbf{T}_{g2l}$ from equation (18).

To use the modal model of the blade segment, we must redistribute the effect of the contact force actuation at point C_i to the profile P_i. Therefore, we must shift the forces to point A_i and substitute moments $F_{tj,i}L$ $(j = y,z)$ by adding force couples $F_{tm,i} = \pm F_{tj,i}L/l$ to points A_i, B_i, where l is the distance between these points. Because the two contact pairs act on each profile, the total forces will be

$$F_{Atj,i} = -F_{tj,i} + F_{tmj,i} + F_{tj,i-1}, \quad F_{Btj,i} = -F_{tmj,i} \tag{20}$$

at points A_i and B_i, respectively.

Then vector ${}^{\mathrm{T}}\mathbf{f}_{cRt} = \left[{}^{\mathrm{T}}\mathbf{f}_{cRt1} \quad {}^{\mathrm{T}}\mathbf{f}_{cRt2} \quad \dots \quad {}^{\mathrm{T}}\mathbf{f}_{cRtn}\right]$ from equation (13) is composed of reduced frictional forces $\mathbf{f}_{cRti} = {}^{\mathrm{T}}\overline{\mathbf{X}}\mathbf{b}_{cFi}$ of each blade $(i = 1,\ n_r)$ where frictional force distribution vector $\mathbf{b}_{cFi}$ is dependent both on arm placement and values of total contact forces acting on the blade.

5. BLADED WHEEL MODEL DESCRIPTION AND RESULTS

The numerical models of the whole wheel with its mesh of 1 946 303 nodes and the one-blade segment used for an MSM of 30 383 nodes (91 149 DOFs) were built in the program ANSYS 19.3. The node topology of one-blade segment including blade and disc partition is shown in Fig. 7. In addition, the nodes (N25201 and N25467) of y-axis nozzle excitation are depicted here, too. The bottom nodes (light blue marks) of the model (shaft area) were clamped in all DOFs. The couplings of 50 disc-node pairs between the left and right sides of neighbouring segments lie on the red lines (Fig. 6). All DOFs of the paired nodes were connected by springs with stiffness $c_1 = 2\text{e}8$ N/m. Then the modification matrix $\Delta\mathbf{K}_{cR}$ from equation (12) was created. Since the modal matrix $\overline{\mathbf{X}} \in \mathbb{R}^{91149\times 10}$ consisted of eigenmodes of the first ten eigenfrequencies of the segment, the final dimensions of the global matrices of equation (12) were reduced (660x660). Modal reduction of the one-blade segment and MSM of the wheel were performed in the MATLAB program. Time response simulations of the bladed wheel were realized in Simulink using the 'ode3' fixed step solver with time step 5e-6s.

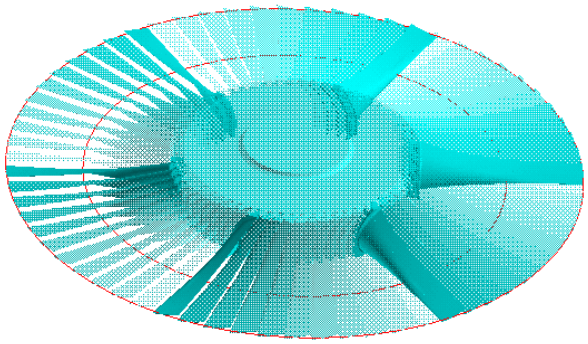

Fig. 6. ANSYS model of bladed wheel with blade interconnections (red lines)

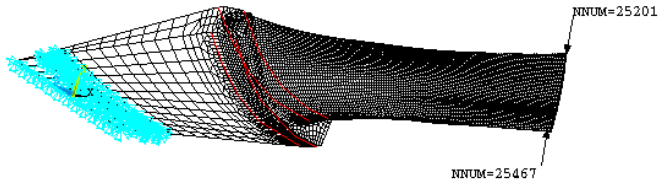

Fig. 7. FE model of a single blade segment

By coupling between the 1st and the last (66th) blade, we create a rotational periodicity of the assembly. These structures are characterised by double eigenfrequencies of the eigenvalue problem.

The specifications of the tie-bosses and contact surfaces:

- Arms of the tie-bosses and shrouds are placed at height $H = H_1$ (tie-boss) and H_2 (shroud), respectively, from the axis of the wheel shaft;
- arms are rigid, massless 1D elements of length $L = L_1$ (tie-boss) and L_2 (shroud), respectively;
- thickness of profile $l = l_1$ (tie-boss) and l_2 (shroud), respectively;
- arms are perpendicular to radial axis (x) of the bladed wheel (a small slope of $5.5^\circ = 360/66$ blades is negligible);
- contact surface angles $\beta_i = \beta_{i,1}$ (tie-boss) and $\beta_{i,2}$ (shroud), respectively.

Parameters of the computational model are written in Table 1.

Table 1
Table of simulation parameters

	parameter	value	unit
blades	n_r	66	
	n_s	64	
revolution	f_{rev}	50	Hz
Van der Pol	r	5e-3	m
	μ	100	Nsm^{-1}
damping	β_D	5e-8	
dry friction	f_s	0.6	
	f_d	0.4	
	d	2	
	v_k	0.6	ms^{-1}
tie-boss	F_{n1}	400	N
	H_1	1.6	m
	β_1	45	$^\circ$
	k_{c1}	7.6e7	N/m
	L_1	0.15	m
	l_1	3.1e-2	m
shroud	F_{n2}	400	N
	H_2	2.18	m
	L_2	0.2	m
	l_2	3.46e-2	m

To evaluate the accuracy of the MSM method, we calculated the first mode families, i.e., axial and tangential blade modes with zero nodal circles, of eigenfrequencies of the bladed wheel without inter-blade arms, see Fig. 8, ascertained by MSM and full 3D finite element model. Both methods show very good mutual agreement. The modal analysis was evaluated for revolution speed 3000 rpm. The eigenfrequency characteristics of both families are quite flat due to very stiff disc. The 5 ND axial bending mode, the 10-th by order number, is depicted in Fig. 9.

Transient bladed disc responses on nozzle and Van der Pol excitations are studied herein for one fixed angle of the contact surfaces in tie-bosses, i.e., $\beta_{i,1} = 45^\circ$, and gradually changing the contact angles $\beta_{i,2}$ in step 5° within the interval $[0, 90]^\circ$ in the shroud. The nozzle excitation of each blade is driven by harmonic function equation (13) with nozzle frequency and phase angle given by the ratio between stator and rotor blades.

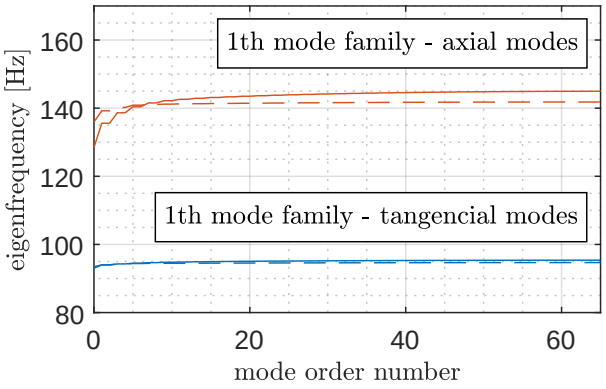

Fig. 8. Calculated eigenfrequency versus mode order number characteristics for the reduced wheel model (dashed) and full wheel model (solid lines) at 3000 rpm: 1st family of tangential modes (blue) and axial modes (red colour)

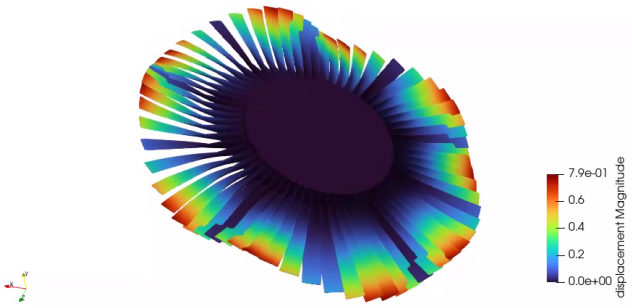

Fig. 9. 5 ND axial bending mode

Time dependencies of maximal vibration amplitudes of blade tips (Fig. 10) and normal contact forces at tie-boss and shroud contacts (Fig. 11) were evaluated in time resolution 37.5 ms, i.e., in a time less than that of two revolutions at 3000 rpm during simulations and are shown in graphs. It can be seen that for angles $\beta_{i,2}$ in the interval $[50, 55]^\circ$ the dry-friction damping sufficiently suppresses the self-excitation with a small variance of

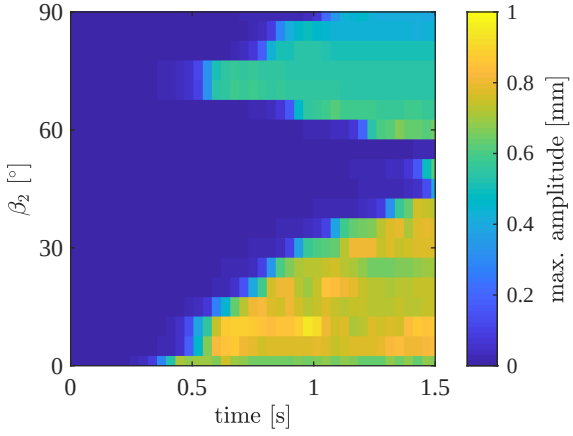

Fig. 10. Dependence of vibration amplitudes of the blades on the angle of shroud contact surfaces in time

normal contact forces. For angles out of this interval, the amplitudes increase and the vibration reaches a state of self-excited vibration. In addition, the contact normal forces drop to zero, leading to loss of contacts and risk of impact in the contacts. The loss of contacts causes a lowering of the dry friction damping as well. This decrease in the normal force does not have to appear in the shroud and tie-boss at the same time, as seen in $\beta_{i,2}$ greater than 60° when only normal forces in tie-boss get into zero.

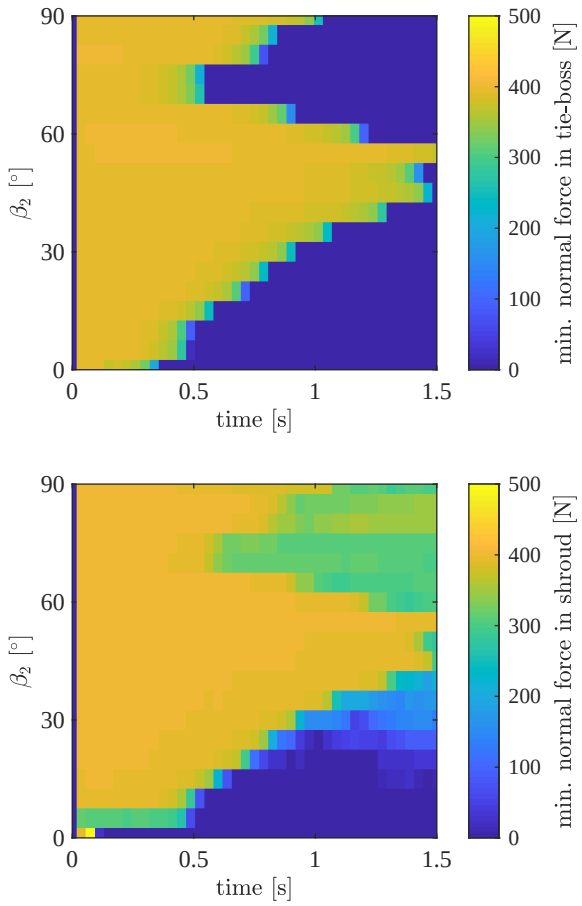

Fig. 11. Dependence of minimal normal forces in contacts on the angle of contact surfaces in time: tie-boss (upper), shroud (bottom)

To better understand the dynamics of the bladed wheel during excitation, FFTs of displacements of all 66 blades for two contact angles $\beta_{i,2}$: A) 55°; B) 20° were calculated and plotted (Fig. 12) in each evaluation step. This evaluation helps to determine the excited vibration modes by number of nodal diameters (NDs). In both cases there is seen mode of 2 NDs from the very beginning of the simulation. It is due to the nozzle excitation that excites the mode of ND equal to difference in numbers of stator and rotor blades ($n_s - n_r = 2$). However, this mode does not get to self-excitation in case A) but it triggers an excitation of other modes in a longer integration time but still at reasonable levels. In the B) case, more modes are dominantly excited, e.g. 0 ND, 25-33ND, that get into a high vibration amplitudes. Excited modes are scattered almost in all ranges of NDs.

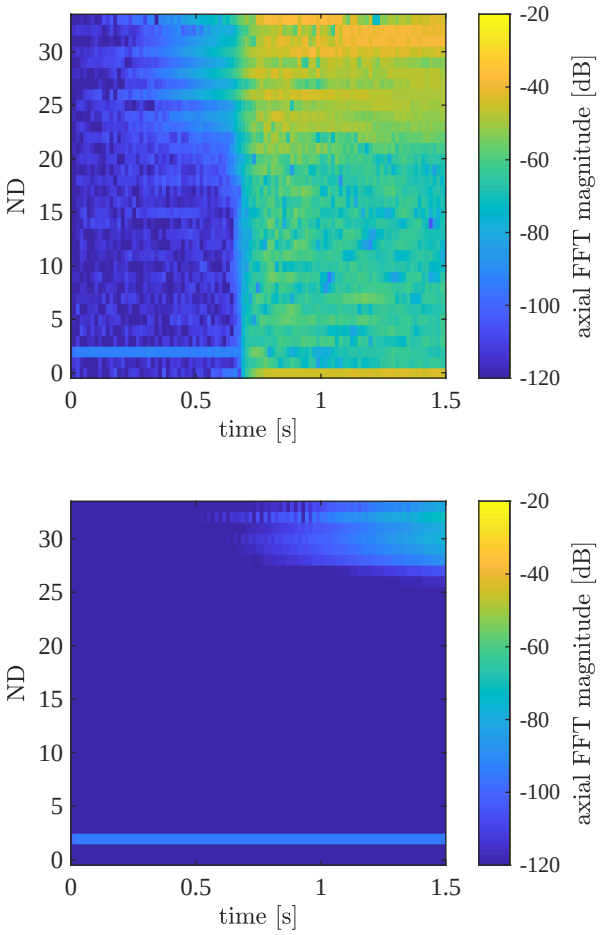

Fig. 12. Mode shape of the wheel vibration characterized by number of NDs: $\beta_{i,2} = 55°$ (upper), $\beta_{i,2} = 20°$ (bottom)

6. CONCLUSIONS

A modal synthesis method as a ROM method is proposed as analytical tool for the study of dry-friction effects of inter-blade connections on the turbine-bladed wheel at self-excitation due to aeroelastic instabilities. This approach enables us to make a numerically effective analysis of the connection parameters, such as placement, arm length, contact surface angles, etc. The numerical simulation of the transient response of the wheel for one set of contact angles takes about a half-hour on a regular PC, which is drastically less than the computation time which would take several weeks of high-performance computing for an unreduced 3D FE nonlinear solution with dry-friction contacts at required integration times [14]. To demonstrate the method, we chose one special case of a turbine wheel with tie-boss and shroud connections. Results of the bladed disc responses are studied for one fixed angle of the contact surfaces in tie-bosses and gradually changing the contact angles in the interval [0, 90]° in the shroud. It can be seen that for the shroud contact angles in interval [50, 55]° the dry-friction damping sufficiently suppresses the self-excitation with a small variance of normal contact forces in a short time (1.5 s) interval of observation. Nowadays we deal with flutter development in longer simulation times. Contrary to the previous form of Van

der Pol model controlled by absolute motion of a profile, the dry-friction damping at the right choice of the contact angles can much better stabilize the self-excitation.

ACKNOWLEDGEMENTS

This work was supported by the research project of the Czech Science Foundation Study of dynamic stall flutter instabilities and their consequences in turbomachinery application by mathematical, numerical and experimental methods [No. 20-26779S].

REFERENCES

[1] J. Rao, *Turbomachine blade vibration*. New Age International, 1991.

[2] W. Sextro, *Dynamical contact problems with friction*. Springer, 2007, doi: 10.1007/978-3-540-45317-8.

[3] A. Muszyńska and D. Jones, "Bladed disk dynamics investigated by a discrete model: effects of traveling wave excitation friction and mistuning," in *Proc. of the Machinery Vibration Monitoring and Analysis Meeting*, vol. 49, 1982.

[4] A. Muszyńska and D. Jones, "On tuned bladed disk dynamics: Some aspects of friction related mistuning," *J. Sound Vib.*, vol. 86, no. 1, pp. 107–128, 1983, doi: 10.1016/0022-460X(83)90947-1.

[5] A. Muszyńska and D. Jones, "A parametric study of dynamic response of a discrete model of turbomachinery bladed disk," *ASME J. Vib. Acoust. Stress Reliab.*, vol. 105, pp. 434–443, 1983, doi: 10.1115/1.3269125.

[6] A. Francavilla and O. Zienkiewicz, "A note on numerical computation of elastic contact problems," *Int. J. Numer. Methods Eng.*, vol. 9, no. 4, pp. 913–924, 1975, doi: 10.1002/nme.1620090410.

[7] P. Wriggers, T. V. Van, and E. Stein, "Finite element formulation of large deformation impact-contact problems with friction," *Comput. Struct.*, vol. 37, no. 3, pp. 319–331, 1990, doi: 10.1016/0045-7949(90)90324-U.

[8] J.C. Simo and T. Laursen, "An augmented lagrangian treatment of contact problems involving friction," *Comput. Struct.*, vol. 42, no. 1, pp. 97–116, 1992, doi: 10.1016/0045-7949(92)90540-G.

[9] J. Awrejcewicz and Y. Pyr'yev, "Nonsmooth dynamics of contacting thermoelastic bodies," ser. Advances in Mechanics and Mathematics. Springer, 2008, vol. 16, doi: 10.1007/978-0-387-09653-7.

[10] M. Wiercigroch and B. De Kraker, *Applied nonlinear dynamics and chaos of mechanical systems with discontinuities*, ser. World Scientific Series on Nonlinear Science Series A. World Scientific, 2000, vol. 28, doi: 10.1142/3345.

[11] L. Pešek and L. Půst, "Blade couple connected by damping element with dry friction contacts," *J. Theor. Appl. Mech.*, vol. 52, no. 3, pp. 815–826, 2014.

[12] N. Bachschmid, S. Bistolfi, M. Ferrante, P. Pennacchi, E. Pesatori, M. Sanvito *et al.*, "An investigation on the dynamic behavior of blades coupled by shroud contacts," *Proc. SIRM*, pp. 1–10, 2011.

[13] P. Pennacchi, S. Chatterton, N. Bachschmid, E. Pesatori, and G. Turozzi, "A model to study the reduction of turbine blade vibration using the snubbing mechanism," *Mech. Syst. Signal Process.*, vol. 25, no. 4, pp. 1260–1275, 2011, doi: 10.1016/j.ymssp.2010.10.006.

[14] L. Pešek, F. Vaněk, J. Veselý, V. Bula, and J. Cibulka, "Design of test excitation of traveling waves of rotating bladed wheels with multipoint electromagnetic excitation," in *Proc. of 9th international conference on vibrations in rotating machines*, 2011, pp. 1–11.

[15] Y. Yamashita, K. Shiohata, T. Kudo, and H. Yoda, "Vibration characteristics of a continuous cover blade structure with friction contact surfaces of a steam turbine," in *10th Int. Conf. on Vibrations in Rotating Machinery*, 2012, pp. 323–332.

[16] L. Pešek, L. Půst, V. Bula, F. Vaněk, and J. Cibulka, "Inter-slip damping of twisted blades in opposed bundles under rotation," in *10th Int. Conf. on Vibrations in Rotating Machinery*, 2012, pp. 293–302.

[17] L. Pešek, L. Půst, V. Bula, F. Vaněk, and J. Cibulka, "Investigation of dry friction effect of shroud damping wire on model test bladed wheel," in *International Design Engineering Technical Conferences and Computers and Information in Engineering Conference*, vol. 55997, 2013, p. V008T13A050, doi: 10.1115/DETC2013-12851.

[18] L. Pešek, L. Půst, V. Bula, and J. Cibulka, "Numerical analysis of dry friction damping effect of tie-boss couplings on three blade bundle," in *International Design Engineering Technical Conferences and Computers and Information in Engineering Conference*, vol. 58226, 2017, p. V008T12A029, doi: 10.1115/DETC2017-67118.

[19] R. Drozdowski, L. Völker, M. Häfele, and D. Vogt, "Experimental and numerical investigation of the nonlinear vibrational behavior of steam turbine last stage blades with friction bolt damping elements," in *Turbo Expo: Power for Land, Sea, and Air*, vol. 56796, 2015, p. V008T26A007, doi: 10.1115/GT2015-42244.

[20] K. Magnus, K. Popp, and W. Sextro, *Schwingungen*. Springer, 1976, doi: 10.1007/978-3-8348-2575-9.

[21] E. Petrov, "Method for direct parametric analysis of nonlinear forced response of bladed disks with friction contact interfaces," *J. Turbomach.*, vol. 126, no. 4, pp. 654–662, 2004, doi: 10.1115/1.1776588.

[22] E. Petrov, "Method for sensitivity analysis of resonance forced response of bladed disks with nonlinear contact interfaces," *J. Eng. Gas Turbine Power*, vol. 131, no. 2, p. 022510, 2009, doi: 10.1115/1.2969094.

[23] K.Y. Sanliturk, M. Imregun, and D.J. Ewins, "Harmonic Balance Vibration Analysis of Turbine Blades With Friction Dampers," *J. Vib. Acoust.*, vol. 119, no. 1, pp. 96–103, 1997, doi: 10.1115/1.2889693.

[24] S. Zucca, C. M. Firrone, and M. M. Gola, "Numerical assessment of friction damping at turbine blade root joints by simultaneous calculation of the static and dynamic contact loads," *Nonlinear Dyn.*, vol. 67, pp. 1943–1955, 2012, doi: 10.1007/s11071-011-0119-y.

[25] M. Barboteu, D. Danan *et al.*, "Analysis of a dynamic viscoelastic contact problem with normal compliance, normal damped response, and nonmonotone slip rate dependent friction," *Adv. Math. Phys.*, vol. 2016, p. 1562509, 2016, doi: 10.1155/2016/1562509.

[26] D. Süß, M. Jerschl, and K. Willner, "Adaptive harmonic balance analysis of dry friction damped systems," in *Nonlinear Dynamics, Volume 1: Proceedings of the 34th IMAC, A Conference and Exposition on Structural Dynamics 2016*, 2016, pp. 405–414, doi: 10.1007/978-3-319-29739-2_36.

[27] J. Voldřich, J. Lazar, P. Polach, and Š. Morávka, "Finding the stiffnesses of interface contact elements for the computational model of steam turbine blading," in *International Design Engi-*

neering Technical Conferences and Computers and Information in Engineering Conference, vol. 58226, 2017, p. V008T12A018, doi: 10.1115/DETC2017-67712.

[28] L. Pešek, M. Hajžman, L. Půst, V. Zeman, M. Byrtus, and J. Brůha, "Experimental and numerical investigation of friction element dissipative effects in blade shrouding," *Nonlinear Dyn.*, vol. 79, pp. 1711–1726, 2015, doi: 10.1007/s11071-014-1769-3.

[29] V. Zeman and Z. Hlaváč, "Generalized modal reduction method for the dynamic analysis of rotating mechanical systems," *Appl. Comput. Mech.*, vol. 14, no. 1, pp. 81–98, 2020.

[30] L. Pešek, P. Šnábl, and V. Bula, "Dry friction interblade damping by 3d fem modelling of bladed disk: Hpc calculations compared with experiment," *Shock Vib.*, vol. 2021, p. 5554379, 2021, doi: 10.1155/2021/5554379.

[31] H. Atassi and T. Akai, "Effect of blade loading and thickness on the aerodynamics of oscillating cascades," in *16th Aerospace Sciences Meeting*, 1978, p. 227, doi: 10.2514/6.1978–227.

[32] J. Panovsky and R. Kielb, "A design method to prevent low pressure turbine blade flutter," *J. Eng. Gas Turbines Power*, vol. 122, no. 1, pp. 89–98, 2000, doi: 10.1115/1.483180.

[33] D. Vogt, "Experimental investigation of three-dimensional mechanisms in low-pressure turbine flutter," Ph.D. dissertation, KTH, School of Industrial Engineering and Management (ITM), Energy Technology, 2005. [Online]. Available: https://www.diva-portal.org/smash/get/diva2:7902/FULLTEXT01.pdf

[34] F. Barbarossa, A.B. Parry, J.S. Green, and L. di Mare, "An aerodynamic parameter for low-pressure turbine flutter," *J. Turbomach.*, vol. 138, no. 5, p. 051001, 2016, doi: 10.1115/1.4032184.

[35] P. Petrie-Repar, V. Makhnov, N. Shabrov, E. Smirnov, S. Galaev, and K. Eliseev, "Advanced flutter analysis of a long shrouded steam turbine blade," in *Turbo Expo: Power for Land, Sea, and Air*, vol. 45776, 2014, p. V07BT35A022, doi: 10.1115/GT2014-26874.

[36] C. Fuhrer and D.M. Vogt, "On the impact of simulation approaches on the predicted aerodynamic damping of a low pressure steam turbine rotor," in *Turbo Expo: Power for Land, Sea, and Air*, vol. 50954, 2017, p. V008T29A007, doi: 10.1115/GT2017-63401.

[37] T. Tanuma *et al.*, "Aerodynamic and structural numerical investigation of unsteady flow effects on last stage blades," in *Turbo Expo: Power for Land, Sea, and Air*, vol. 56796, 2015, p. V008T26A035, doi: 10.1115/GT2015-43848.

[38] V. Slama, B. Rudas, J. Ira, A. Macalka, P. Eret, and V. Tsymbalyuk, "Subsonic stall flutter of a linear turbine blade cascade using experimental and cfd analysis," in *ASME International Mechanical Engineering Congress and Exposition*, vol. 84546, 2020, p. V07AT07A026, doi: 10.1115/IMECE2020-23356.

[39] A. Laksana, A. Kokong, P.A. Sigit, T. Widjajanto, H. Setiawan, and I. Djunaedi, "Flutter analysis of last stage steam turbine power plant blade through transient blade row simulation," in *IOP Conference Series: Materials Science and Engineering*, vol. 1096, no. 1, 2021, p. 012093, doi: 10.1088/1757-899X/1096/1/012093.

[40] L. Pinelli *et al.*, "Aeromechanical characterization of a last stage steam blade at low load operation: Part 2—computational modelling and comparison," in *Turbo Expo: Power for Land, Sea, and Air*, vol. 84218, 2020, p. V10AT24A017, doi: 10.1115/GT2020-15409.

[41] C. Prasad, P. Šnábl, P. Procházka, and S. Chindada, "Effect of geometrical and flow parameters on subsonic stall flutter in blade cascade," in *Proc. 19th Int. Forum Aeroelasticity and Structural Dynamics*, 2022.

[42] C.S. Prasad, P. Šnábl, and L. Pešek, "A meshless method for subsonic stall flutter analysis of turbomachinery 3D blade cascade," *Bull. Pol. Acad. Sci. Tech. Sci*, vol. 69, no. 6, p. e139000, 2021.

[43] C.S. Prasad, R. Kolman, and L. Pešek, "Meshfree reduced order model for turbomachinery blade flutter analysis," *Int. J. Mech.*, vol. 222, p. 107222, 2022.

[44] C.S. Prasad and L. Pešek, "Analysis of classical flutter in steam turbine blades using reduced order aeroelastic model," in *MATEC Web of Conferences*, vol. 211, 2018, p. 15001, doi: 10.1051/matecconf/201821115001.

[45] D. Su, W. Zhang, and Z. Ye, "A reduced order model for uncoupled and coupled cascade flutter analysis," *J. Fluids Struct.*, vol. 61, pp. 410–430, 2016, doi: 10.1016/j.jfluidstructs.2015.11.013.

[46] J. Panovsky and R.E. Kielb, "A design method to prevent low pressure turbine blade flutter," in *Turbo Expo: Power for Land, Sea, and Air*, vol. 78668, 1998, p. V005T14A052, doi: 10.1115/98-GT-575.

[47] M. Meingast, R.E. Kielb, and J.P. Thomas, "Preliminary flutter design method for supersonic low pressure turbines," in *Turbo Expo: Power for Land, Sea, and Air*, vol. 48876, 2009, pp. 507–515, doi: 10.1115/GT2009-59177.

[48] D.M. Vogt and T.H. Fransson, "A new turbine cascade for aeromechanical testing," in *Proc. of the 16th Symposium on Measuring Techniques in Transonic and Supersonic Flow in Cascades and Turbomachines*, 2002.

[49] P. Eret and V. Tsymbalyuk, "Experimental Subsonic Flutter of a Linear Turbine Blade Cascade With Various Mode Shapes and Chordwise Torsion Axis Locations," *J. Turbomach.*, vol. 145, no. 6, p. 061002, 2022, doi: 10.1115/1.4056204.

[50] V. Sláma *et al.*, "Experimental and numerical study of controlled flutter testing in a linear turbine blade cascade," *Acta Polytechnica CTU Proceedings*, vol. 20, pp. 98—-107, 2018, doi: 10.14311/APP.2018.20.0098.

[51] P. Jutur and R.N. Govardhan, "Flutter in Started and Unstarted Transonic Linear Cascades: Simultaneous Measurements of Unsteady Loads and Shock Dynamics," *J. Turbomach.*, vol. 141, no. 12, p. 121004, 2019, doi: 10.1115/1.4045105.

[52] P. Šidlof, D. Šimurda, J. Lepicovsky, M. Štěpán, and V. Vomáčko, "Flutter in a simplified blade cascade: Limits of the quasi-steady approximation," *J. Fluids Struct.*, vol. 120, p. 103913, 2023, doi: 10.1016/j.jfluidstructs.2023.103913.

[53] L. Pešek, P. Šnábl, and C.S. Prasad, "Reduced modal model of bladed turbine wheel for study of suppression of self-excited vibration by dry- friction contacts," in *Proc. 14th Int. conf. Dynamics of Rotating Machines (SIRM)*, Gdańsk, Poland, 2021, pp. 371–380.

[54] L. Pešek, P. Šnábl, and C.S. Prasad, "Modal synthesis method for inter-blade dry-friction surface angle design of turbine wheel for vibration suppression," in *Proc. Int. Conf. Design Engineering Technical Conferences & Computers and Information in Engineering (IDETC/CIE)*, 2022, p. 9, doi: 10.1115/DETC2022-88382.

[55] J. He, "Structural modification," *Phil. Trans. R. Soc. A.*, vol. 359, pp. 187–204, 2001, doi: 10.1098/rsta.2000.0720.

[56] L. Půst and L. Pešek, "Blades forced vibration under aero-elastic excitation modeled by Van der Pol," *Int. J. Bifurcat. Chaos*, vol. 27, no. 11, p. 1750166, 2017, doi: 10.1142/S0218127417501668.

[57] L. Půst, L. Pešek, and M. Byrtus, "Modelling of flutter running waves in turbine blades cascade," *J. Sound Vib.*, vol. 436, pp. 286–294, 2018, doi: 10.1016/j.jsv.2018.08.011.